Title
Biophysical isolation and identification of circulating tumor cells

Journal
Lab on a Chip, 17(8)

ISSN
1473-0197

Authors
Che, James
Yu, Victor
Garon, Edward B
et al.

Publication Date
2017-04-11

DOI
10.1039/c7lc00038c

Peer reviewed

HHS Public Access

Author manuscript

Lab Chip. Author manuscript; available in PMC 2018 April 11.

Published in final edited form as:

Lab Chip. 2017 April 11; 17(8): 1452–1461. doi:10.1039/c7lc00038c.

Biophysical isolation and identification of circulating tumor cells

James Che[1], **Victor Yu**[1], **Edward B. Garon**[2,3], **Jonathan Goldman**[2,3], and **Dino Di Carlo**[1,3,4,*]

[1]Department of Bioengineering, University of California, Los Angeles, 410 Westwood Plaza, Los Angeles, California, 90095, USA

[2]UCLA Santa Monica Hematology & Oncology, 2020 Santa Monica Blvd, Suite 600, Santa Monica, California, 90404, USA

[3]Jonsson Comprehensive Cancer Center, Los Angeles CA, 90095, USA

[4]California NanoSystems Institute, Los Angeles, California, 90095, USA

Abstract

Isolation and enumeration of circulating tumor cells (CTCs) from blood is important for determining patient prognosis and monitoring treatment. Methods based on affinity to cell surface markers have been applied to both purify (via immunoseparation) and identify (via immunofluorescence) CTCs. However, variability of cell biomarker expression associated with tumor heterogeneity and evolution and cross-reactivity of antibody probes have long complicated CTC enrichment and immunostaining. Here we report a truly label-free high-throughput microfluidic approach to isolate, enumerate, and characterize the biophysical properties of CTCs on an integrated microfluidic device. Vortex-mediated Deformability Cytometry (VDC) consists of an initial vortex region which enriches for large CTCs, followed by release into a downstream hydrodynamic stretching region which deforms the cells. Visualization and quantification of cell deformation with a high-speed camera revealed populations of large (>15 μm diameter) and deformable (aspect ratio >1.2) CTCs from 16 stage IV lung cancer samples, that are clearly distinguished by increased deformability compared to contaminating blood cells and rare large cells isolated from healthy patients. VDC technology demonstrated a comparable positive detection rate of putative CTCs above healthy baseline (93.8%) with respect to standard immunofluorescence (71.4%). Automation allows full enumeration of CTCs from a 10mL vial of blood within <1 hr after sample acquisition, compared with 4+ hours with standard approaches. Moreover, cells are released into any collection vessel for further downstream analysis. VDC shows potential for accurate CTC enumeration without labels and confirms the unique highly deformable biophysical properties of large CTCs circulating in blood.

TOC Image

[*]**Correspondence**: Dino Di Carlo, dicarlo@seas.ucla.edu.

Author contributions: J.C. and D.D. designed research; J.C. and V.Y. performed research and experiments; E.G., and J.G. contributed resources; J.C. analyzed data; J.C., E.G., J.G., and D.D. wrote the paper.

Competing financial interests: J.C. and D.D. have submitted a patent application related to the presented work. J.C. is an employee at Vortex Biosciences, Inc. The Regents of the University of California, J.C., and D.D. have financial interests in Vortex Biosciences, Inc. D. D. and the Regents of the University of California have financial interests in CytoVale, which is commercializing Deformability Cytometry technology.

The integrated Vortex enrichment – Deformability Cytometry device may enable automated enumeration of circulating tumor cells from blood by mechanophenotyping

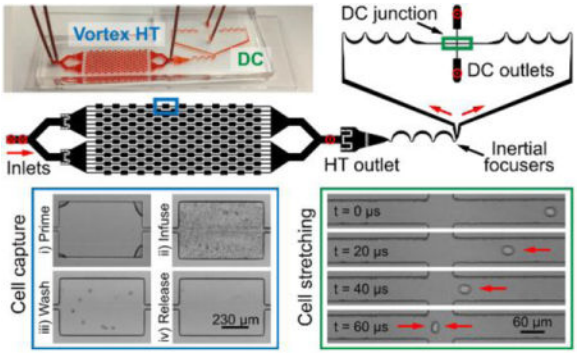

Keywords

label-free detection; mechanophenotyping; circulating tumor cell; rare cell isolation

INTRODUCTION

Circulating tumor cells (CTCs) are rare populations of cells which have shed from a tumor into the blood stream, and are minimally invasive biomarkers of metastatic cancer progression. Enumeration of CTCs from a liquid biopsy has been applied for determining patient prognosis and monitoring treatment.[1,2] Additionally, CTCs may be convenient sources to sample tumor tissue for use in drug discovery, cytopathology, genetic testing for personalized medicine, and other clinical applications.[3] However, CTCs must typically first be i) isolated and enriched from a large background of red and white blood cells (WBCs), and subsequently ii) identified and distinguished from contaminating cells for enumeration and characterization. Rapid identification and enumeration without damaging or altering the cells can be especially useful to distinguish samples with sufficient numbers of diagnostic cells for more costly but information-rich downstream assays, such as sequencing or cytogenetics.

Affinity-based approaches have widely been employed to both isolate and identify CTCs,[4] in which antibodies bind to specific cell surface markers as anchorage for extraction (immunoseparation) or as probes for detection (immunofluorescence). However, variability of biomarker expression, especially for CTCs undergoing epithelial-to-mesenchymal transition (EMT),[5,6] and cross-reactivity of binding have long complicated CTC targeting. One emerging approach to CTC capture is to employ negative depletion,[7] in which blood cells are targeted and depleted from unbound CTCs; nevertheless, all affinity-based capture approaches have typically yielded low sample purities (<1%), causing challenges in downstream analyses such as genotyping. In terms of CTC identification, the use of affinity-based immunofluorescence (IF) has remained the universal gold standard to distinguish captured CTCs for enumeration and assess device performance. Despite inherent complications with specificity and sensitivity of detection, IF also suffers from a lengthy time (>3 hrs) needed for staining, imaging, and manual enumeration per sample, and the

process often harms cells and excludes them from other types of analyses. Ideally, a completely label-free technique would offer a powerful and affordable alternative to assay all types of cells, including those which are positive for epithelial cell adhesion marker (EpCAM), EpCAM-negative, and undergoing EMT. In addition, such a label-free technique opens up the possibility for targeting expensive molecular assays only to patients with high numbers of identified cells.

Aside from the use of antibodies to target heterogeneous surface antigens, gene network-level changes in CTCs may alternatively be encompassed by measurable biophysical parameters, such as cell size and deformability.[8,9] Many emerging microfluidic technologies take advantage of cell size as a means for isolating CTCs,[10] which tend to be larger than their blood cell counterparts.[11] Strategies include the use of pores[12] or narrow channel constrictions[13] for microfiltration, micropillar arrays for deterministic lateral displacement,[14] or dean flow fractionation[15] in which inertial fluidic forces scale strongly with cell size.[16] Depending on the specific downstream applications, certain technologies may be favored over others since many have limitations with capture efficiency, sample purity, throughput, scalability, dilute output volume, cell damage, manually intensive procedures, or other impeding factors.

Increased cell deformability has also been investigated as a marker for more invasive cancer cells. The prevailing hypothesis is that invasive cells are selected to have deformable physical properties associated with the ability to squeeze through tissue and enter the blood stream or lymphatics in order to metastasize to different sites. Initial work in the field evaluated established cell lines and found that deformability increased (e.g. progressing from MCF10A, MCF7, and mod-MCF7 cells) with invasive potential.[17] Later work showed that primary malignant cells in the oral cavity[18] or disseminated in the pleural cavity[19] also possessed a higher deformability than healthy epithelial or mesothelial cells present in those cavities.

Tumor cells circulating in the blood are much rarer than in other body fluids and have been difficult to probe the true physiological state mechanically.[20] Although capture of CTCs in filter structures can depend on cell deformability and size,[11,13] there has been no conclusive study evaluating the mechanical properties of circulating tumor cells as they appear within the blood, in a manner independent of differences in size. In fact, because of cell deformability, many filtration reports require cell fixation prior to processing, preventing characterization of the in vivo biophysical state of CTCs.

Several techniques have been developed to characterize cell deformability,[21] such as measuring the time of cell passage through narrow channel constrictions,[22,23] driving cells through pinched flow streams to measure hydrodynamic stretching,[24,25] using optofluidic laser technology for single-cell stretching and sorting,[17,26,27] magnetic twisting cytometry,[28] micropipette aspiration,[29] and atomic force microscopy (AFM).[19,30] These technologies have been demonstrated on more readily abundant sources of cells such as stem cells,[31] cultured cancer cells,[29] and tumor cells from tissue sections[32] or body cavity fluids.[19,33] However, we found only two limited reports which examined the mechanical properties of 12 total native CTCs from prostate cancer patients using AFM[11] or microchannel

constrictions.[23] The overall rarity and low purity of CTC samples provided by most enrichment techniques also impedes routine single cell biophysical measurements (Fig. 1A), requiring downstream single cell picking and manual processing.[30]

We have previously reported separate label-free inertial microfluidic technologies to isolate and measure cancer cells with a significant level of automation. First, the High-Throughput Vortex Chip (Vortex HT) is a size-selective sample preparation tool that quickly (800 μL/min of whole blood) and passively isolates large CTCs (>13 μm) from blood at high purity (up to 80%), into a small volume (150 μL total), and with reasonable efficiency (~23% per cycle and up to 83% with 6 cycles of reprocessing) and viability (>80%) by making use of stable laminar microvortices.[34] Vortex HT captures more CTCs than the CellSearch gold standard and identifies a higher percentage of non-small cell lung cancer (NSCLC) blood samples as positive for CTCs above a healthy baseline. Second, we also developed the Deformability Cytometry (DC) technique which rapidly images (~2,000 cells/s) and measures the biophysical parameters (e.g. size, deformability) of single cells hydrodynamically stretched in an extensional flow junction.[31,33] However, without prior enrichment of CTCs from blood, and even with RBC lysis this DC technique with automated image processing is too slow to sift through the tens of millions of WBCs.

We expected that the enrichment and analysis of CTCs using the combination of vortex purification and hydrodynamic stretching could uniquely distinguish them from other cell types present in blood, allowing for automated cell enumeration to predict patient outcome in a rapid and cost-effective label-free process. However, device integration is non-trivial because of several fundamental challenges including i) the operational flow rate of the vortex trapping system at 8 mL/min is 10-fold higher than the deformability cytometry system and ii) high-speed imaging required for deformability measurements of cells has a limited window of recording that must be synchronized with the release of cells from vortex traps.

Here we report a monolithically integrated Vortex trapping and Deformability Cytometry system (VDC) and operational process that enabled seamless capture, release, and measurement of rare cells. Following system validation, we applied the system to analyze the mechanical properties of CTCs from 16 stage IV NSCLC patients. We observed increased size and deformability of large cells isolated from cancer patients was a distinguishing characteristic that strongly correlated with immunofluorescence-based counts of CTCs from the same patient, which enabled discrimination from blood cells and facilitated label-free enumeration. The biophysical profiles of CTCs can now be investigated to uncover whether further correlations with patient status, such as staging, cancer type, or response to treatment may exist.

EXPERIMENTAL

Vortex-mediated deformability cytometry layout and working principles

A PDMS device and workflow was developed to integrate the Vortex HT microfluidic design with DC into a streamlined label-free enrichment and enumeration process. The resulting Vortex-mediated Deformability Cytometry (VDC) device (Fig. 1B) consists of two

components: i) a 70μm-deep Vortex HT region consisting of 16 parallel 40μm-wide straight channels passing through 160 total rectangular 480μm × 720μm trapping reservoirs, and ii) a 35μm-deep DC region which hydrodynamically stretches cells at a 60μm × 60μm extensional flow junction. The VDC device has two inlets for PBS wash buffer and sample (Fig. 1C). One outlet is located directly after the Vortex HT region (the HT outlet), through which fluid waste passes at high flow rate during device priming, sample infusion and cell capture, and solution exchange (Fig. 1D, Fig. S1), as described in previous work.[34,35]

Once cells are captured in vortices and excess blood cells are washed away, the HT outlet is briefly closed (~1s), causing a sudden pressure increase that expands the walls of the elastic PDMS reservoirs and disrupt the vortices (Video S1), which is required to rapidly release the cells through the DC region of the device and out either of the two DC outlets. Cells deform at the DC extensional flow junction and are imaged with a high-speed camera synchronized to the release step (Fig. 1E).[31,33] After deformation, cells are flushed from the device into a collection vessel along with a small ~200μL volume of PBS.

Device fabrication

Polydimethylsiloxane (PDMS) devices were assembled using traditional replica molding techniques. Briefly, a 4″ silicon wafer (University Wafer, Inc.) master mold was first fabricated using standard photolithography using a mask (CAD/Art Services, Inc.) designed using AutoCAD (Autodesk, Inc.). KMPR photoresist (MicroChem Corp.) was used in a two-step process to spin, expose, and develop the 35μm-deep DC region and subsequent 70μm-deep Vortex HT region. Regions were aligned before exposure (Karl Suss MA6, SUSS MicroTec AG), and channel heights were confirmed by profilometry (Dektak 6, Veeco Instruments, Inc.). PDMS was mixed in a 1:10 base to crosslinker ratio, poured over the mold, degassed, and baked at 60°C for 21hrs before being cut and peeled from the mold, hole-punched (Syneo, LLC), and bonded with oxygen plasma (800 Micro RIE, Technics Inc.) to a 3″×1″ glass slide (VWR International LLC) using 80W RF power for 30s at 500mTorr.

Device operation and workflow

The specific VDC process flow is outlined in Fig. S1. While the typical prime, infuse, wash, and release steps mirror the cell enrichment procedure for Vortex HT processing,[34,35] a few additional considerations were made for the different outlets. The initial priming step takes place one time before the experiment begins, and uses a low flow rate of PBS buffer through the device to ensure all air bubbles are removed. Next, pressurization occurs at high flow rate with the DC outlets closed, in which the PDMS reservoirs become pressurized as flow fully develops and exits the HT outlet. This step ensures no residual blood cells will enter the DC region of the device during sample infusion. The blood is then infused through the device at an overall 8mL/min, and large cells become trapped in vortices as fluid waste passes through the HT outlet. Next, the solution is exchanged to buffer at the same flow rate to ensure that trace blood cells are washed away while large cells are stably maintained in vortices (Fig. 1D). Subsequent stabilization, by releasing pressure from the sample syringe, is needed to prevent residual flow and shedding of blood cells through the reservoirs during the wash. During this time, the DC outlets are opened and guided to the well plate. Captured

cells are then released to the DC region occurs by closing the HT outlet, and video recording is triggered at the same time. Finally, cells are flushed from the device at a low flow rate to a collection vessel.

The DC region contains asymmetric curving channels which make use of Dean vortices to first inertially focus and direct cells toward one side of the device, and then focus cells to a single stream in which they may be oriented toward the center of the channel prior to the DC junction. Cells deform at the extensional flow junction and are imaged with a high speed camera at 100× magnification with a Phantom v711 high speed camera (Vision Research) at 511,278fps and 208×32pixel resolution (Fig. 1E), as described in previous work.[31,33]

Device characterization with cell lines

Device performance was characterized using the MCF7 breast cancer cell line (ATCC) as a model for large CTCs and to better compare with previous characterizations of Vortex enrichment in Che et. al., 2016.[34] Briefly, cells were cultured in media consisting of DMEM supplemented with 10% fetal bovine serum, 1% penicillin-streptomycin-glutamine, and 0.01mg/mL human recombinant insulin (Gibco), and incubated at 37°C and 5% CO_2. Cells were detached with 0.25% (w/v) trypsin (HyClone), resuspended in media, and rocked gently for 15min on a shaker before experiments. Efficiency tests were performed by diluting MCF7 cell suspensions to a low working concentration in PBS or 10× diluted healthy blood. A target number of ~300 cells were infused through the VDC device using syringe pumps (Harvard Apparatus PhD 2000). Efficiency was calculated as the number of MCF7 cells captured over the total number of MCF7 cells infused through the device, and purity was defined as the number of MCF7 cells over the total number of nucleated cells in the purified sample. Cells collected in 96-well plates for viability tests were centrifuged, incubated with media, and stained with Calcein AM and ethidium homodimer (Molecular Probes) on separate wells each day over the course of 6 days, at which the experiment was stopped.

Sample collection and analysis

Clinical blood samples were acquired in 10mL EDTA-coated Vacutainer tubes (BD) from consenting non-small cell lung cancer (NSCLC) patients from UCLA Santa Monica Oncology and Hematology, following institutional review board protocols (UCLA IRB #11-001798). Samples were de-identified, diluted 10× in PBS, and processed within 4hrs of acquisition.

Cells collected in 96-well plates for IF enumeration were fixed in 4% paraformaldehyde (Electron Microscopy Sciences) for 10min, permeabilized in 0.4% (v/v) Triton X-100 (Research Products International Corp.) for 7min, blocked with 5% goat serum (Invitrogen) for 30min, and stained with DAPI (Molecular Probes), anti CD45-phycoerythrin (BD Biosciences), and an anti cytokeratin (CK)-FITC cocktail for CK CAM5.2 (BD Biosciences), CK3-6H5 (Miltenyi Biotec), and Pan-CK AE1/AE3 (eBioscience) for 40min at room temperature. Entire wells were imaged and stitched at 100× magnification (Zeiss Axio Observer Z1 microscope) using a CoolSnap HQ2 CCD camera (Photometrics). Enumeration and classification of stained cells was performed with the same objective

criteria described previously in Che et *al.*[34] Briefly, the criteria leveraged both fluorescent staining (CK+/CD45−/DAPI+) and cytomorphological characteristics (large nuclear size > 9μm and nuclear-to-cytoplasmic ratio > 0.8) to classify cells as CTCs. Then, samples were defined as positive for CTCs if they had a total CTC count higher than the maximum count observed from healthy samples (0.125 CTCs/mL threshold).

Video and deformability analysis

A MATLAB (The Mathworks, Inc.) script was developed for automated image analysis to detect cellular events in videos. A user interface was developed to subsequently measure and record size and deformability of each isolated cell. Parameters of size and deformability from the cells of both healthy and cancer patient samples were inputted into a support vector machine function (svmtrain) in MATLAB to define a threshold which distinguishes CTCs from non-CTCs. Specific support points which defined the threshold are shown in Figure S5. The threshold defined in this manner for VDC (by size and deformability) is different from the one defined by IF staining (by the max CTC count from healthy samples). However, thresholding for either method was tuned and implemented to ensure a 0% false positive rate.

RESULTS AND DISCUSSION

VDC device characterization and performance

Captured MCF7 cells are released from the vortices in a quick ~0.5s time interval (Fig. 2A) and also immediately pass through the DC junction within a ~0.5s time frame (Fig. 2B), which is crucial for resolving all cells in one ~1.34s total duration high-speed video. Upon release from the vortices, 98.7% ± 1.5% (n=4) of cells transfer from the Vortex HT region to the DC region (Fig. 2C), which demonstrates minimal cell loss between capture and assay regions. Moreover, the number of cells observed in the DC junction matches closely with the number of cells released into a well plate, indicating minimal cell loss between VDC and downstream collection; as such, the measured efficiency from VDC detection and well plate collection both yields a 25–35% capture efficiency of MCF7 cells spiked in 10× diluted blood and processed through 1 cycle (Fig. 2D). Collected sample purity remained quite high at 35.1% ± 7.3% (n=3), which is important for downstream assays that are hindered by the presence of background wild-type cells. Cells passing through the DC junction maintain an average speed of 4.74 ± 0.93m/s (n=3), which is sufficient to observe and measure deformability (Fig. 2E), defined in this study as the maximum length ratio between the long axis and short axis of the cell. Additionally, collected cells could be grown in culture for >6 days (Figs. 2F, S2), which may be crucial for live-cell studies such as RNA sequencing, drug screening, and metabolic assays. Interestingly, apparent cell viability was low (20%) immediately after collection but recovered (56%) before cell proliferation was observed (Fig. S2), suggesting that VDC process may permeabilize cells to an extent where the ethidium homodimer dead stain indicator may be absorbed. The phenomenon is likely caused at the deformability cytometry segment of the device, where cells may experience shear-induced permeabilization in the extensional flow. Although the stress on cells may affect downstream examinations such as drug screening, and proliferation, and RNA assays,

further investigation will be needed to uncover the short- and long-term effects of VDC on cells post-analysis.

Identification of CTC subpopulations from patient samples

16 stage IV NSCLC and 5 healthy blood samples were processed through VDC (Table S1). Each sample yielded a unique cellular biophysical profile which may be represented as a scatterplot of deformability versus size (Figs. S3, S4). Combining the profiles from all healthy (Fig. 3A) versus all NSCLC (Fig. 3B) samples reveals distinct populations of cells. In both sample types, a population of small 10μm WBCs with average ~1.2 deformability was present. Additionally, a scattered group of larger (>15μm) and more rigid (<1.2) cells was observed in both sample types, which may represent large WBCs (e.g. monocytes) or other large circulating cells (e.g. epithelial cells sloughed off during the blood draw, endothelial progenitor cells, etc.). Finally, a unique population of large (>15μm) and deformable (>1.2) cells was observed only from cancer patient blood samples, suggesting that they are CTCs or cancer-associated cells. By setting user-guided cutoffs for both size and deformability, the dataset was calibrated by support vector machine (SVM) to define a biophysical threshold which defined a putative CTC (Figs. 3C, S5). Based on the threshold, cells were categorized into CTC and WBC groupings. The technique identified 93 CTCs from VDC videos, which tended to be larger and more deformable (Fig. 3D–F, Video S2) than the 584 measured WBCs. CTCs had similar deformability and size ranges as MCF7 cells (Fig. 3G). Similar to observations from preliminary tests with the MCF7 cells, CTCs and WBCs passed through the DC junction in a short <1s time period (Fig. S6A). No correlations between the time of release and the measured deformability were observed (Fig. S6B), suggesting no quantitation bias with the timing of cell events observed in video capture. A small correlation was observed between time of release and cell size (Fig. S6C), which matched experimental observations that larger cells were more favorably captured upstream and consequently exhibited a longer time of travel upon release.

Comparison of VDC measurements with immunofluorescence (IF)

The same cells assayed through VDC from each patient were also collected off-chip and stained for CK (CTC), CD45 (WBC), and DAPI (nucleus) to verify the presence of CTCs by standard IF enumeration protocols and correlate to DC measurements. In the first 9 samples processed, the “stabilize” step (Fig. S1) during processing had not been fully implemented. As a result, a large number of white blood cells were released into the well plates after VDC recording and during the device flushing step prior to the staining process, causing a significant mismatch in WBC numbers between VDC and IF processes (Table S1). Thereafter, implementing the stabilization procedure allowed much fewer WBCs to be shed into the well plate (avg. 28 ± 23 WBCs per mL of blood processed).

Populations of both CK+/CD45−/DAPI+ and large CK−/CD45−/DAPI+ CTCs were present from samples processed by VDC (Fig. 4A). 47% of CTCs stained negative for CK, which is of similar proportion as observed previously in Che *et al.*[34] for NSCLC clinical samples and other studies which explore epithelial-antigen-dependent and -independent techniques.[36] The number of putative CTCs defined from VDC thresholding correlates strongly with the number of CTCs identified by IF (Fig. 4B, R^2=0.987). Additionally, the size distributions

matched well between VDC-defined CTCs and IF-defined CTCs (Fig. 4C), suggesting that the large, deformable population of cells from VDC are indeed CTCs. No correlations were observed between the average deformability, size, and nuclear-to-cytoplasmic ratios of cells observed in VDC and IF (Fig. S7).

Finally, when enumerating CTCs per patient VDC finds 93.8% of NSCLC patient samples positive for CTCs using a biophysical thresholding technique, whereas IF techniques find approximately 71.4% of samples positive for CTCs (Fig. 5) above a healthy threshold. To note, the IF positive test rate fell within 10% of the previously reported rate (80%) which used a larger sample set and the same Vortex HT isolation method.[34] If the IF threshold cutoff (0.13 CTCs/mL) was used to set a baseline threshold for CTCs defined by VDC, 75% of cancer samples identified from VDC would be positive for CTCs. The use of multiparameter biophysical thresholding and cutoffs may thus be a comparable method to IF for defining CTCs and distinguishing between cancer and healthy samples. Further long-term studies with a larger cohort of patients is needed to support these preliminary findings. Nevertheless, biophysical characterization of cells may be a viable alternative to immunofluorescence for future enumeration.

CONCLUSION

We demonstrate to our knowledge the first platform which directly couples CTC enrichment with biophysical quantitation for cell identification. The presence of large cells in healthy samples indicates that cell diameter alone is an insufficient parameter to distinguish CTCs. Coupled with mechanical phenotyping, VDC technology factors both size and deformability in a truly label-free, streamlined, and sensitive method that rapidly extracts and enumerates cells from NSCLC blood samples, while only requiring one blood dilution preparation step. We find evidence that the putative CTC population we collect are large and deformable, since i) only samples from cancer patients contained that population of cells, ii) the number of cells biophysically identified in this manner matched closely with the number of CTCs identified with IF from the same samples, and iii) the size distributions of CTCs matched closely between VDC and IF from the same samples. Nevertheless, there may still exist relatively smaller and/or stiffer CTCs in patient blood that this technology overlooks, especially since Vortex enrichment fundamentally targets large cells.

The true biophysical nature of CTCs has remained elusive. Whereas some have posited that CTCs have low deformability[13,37] and may need to maintain a more solid-like state, potentially to lodge in the microcirculation of particular peripheral sites,[28] many studies have suggested CTCs should be more deformable than normal cells,[18,38–42] potentially as a requirement for intravasation or even for resisting immune responses from mediators such as cytotoxic T lymphocytes which employ synaptic forces to accelerate targeted cell death.[43] Our findings are similar with the latter and Chen *et al.*[30], who show that 4 primary prostate cancer CTCs displayed highly deformable phenotypes, characteristic of high metastatic potential. Although CTC deformability may be determined by a variety of factors, including cytoskeletal (vimentin, actin, microtubules, etc.[44]) and nuclear (heterochromatin, euchromatin, lamins, etc.) composition,[45] response to treatment,[40,46] cancer type,[42,44] the fluid microenvironment,[47] and the particular quantification technique employed, the

differences between CTCs may still be small in comparison to blood cells. Work by Bagnall *et al.*[23] suggested that 8 observed large primary CTCs behaved biophysically similar to blood cells, but they were limited by the operational cell size range their device could accommodate and could not make definitive biophysical comparisons. In contrast, the high fidelity of VDC allows such properties between CTCs and healthy cells to be distinguished, enabling enumeration in a step towards patient prognosis and treatment monitoring.

Other unique alternatives to IF are emerging for CTC detection, including the use of surface plasmon resonance,[48] surface enhanced raman spectroscopy,[49] ultrasound and photoacoustics,[50] electrochemical aptasensors,[51] silicon nano-wire-array detection of magnetic upconversion nanoparticles,[52] light addressable potentiometric sensors,[53] impedance-based detection,[54] and PCR-based methods.[55,56] However, VDC remains a top candidate as a truly label-free enrichment and enumeration platform, supported with preliminary tests using clinical samples. Integration of two high-throughput inertial microfluidic technologies minimizes loss of valuable, rare cells and reduces manual labor, time, and costs. Enumeration data may be outputted within 1 hr from acquisition of a patient sample, whereas traditional techniques require a minimum of 3 hours to purify, immunostain, image, and enumerate CTCs from each sample. Moreover, the number of released CTCs is determined without the need for cell fixation, staining, or other processes that would damage the output sample, allowing viable cells to be usable for downstream analysis, such as cell culture, molecular analysis, drug screening, cytopathology, and other applications in both research and clinical settings. Importantly, the low up-front costs for biophysical enumeration could serve a pre-screening role, allowing for the selection of samples with larger numbers of candidate cells that are likely to yield high quality downstream analyses before investing significant time and resources.

Demonstration of this technology also opens opportunities for future work. First, the Vortex HT component of VDC only selects for large CTCs, and catering biophysical assessment toward smaller CTCs or those of a certain surface antigen may be useful. Next, the transient responses (i.e., strain rate, etc.) and morphology of each cell at the VDC flow junction provides additional biophysical parameters that may further distinguish different cell types or cells undergoing functional changes surrounding proliferation,[44] differentiation,[31] motility,[57] or metastatic potential.[17,28] Additional analysis of CTC biomechanics may thus reveal physical phenotype distributions that are better diagnostic and prognostic indicators of patient state than simple enumeration. Moreover, application of the technology to other cancer types beyond NSCLC may further uncover unique biophysical spaces. Finally, the demonstration of direct coupling between Vortex CTC enrichment and downstream technologies may prove useful for linking to other platforms for alternative modes of single-cell analyses,[58] such as with droplet microfluidics for cell metabolomic,[59] genomic,[60] or proteomic assays.[61]

Supplementary Material

Refer to Web version on PubMed Central for supplementary material.

Acknowledgments

We thank Melissa Matsumoto for patient sample collection and all blood donors for contributions to the work. We also thank Jonathan Lin and Hector Enrique Muñoz for initial guidance with deformability cytometry, and the UCLA Nanoelectronics Research Facility for access to microfabrication facilities. This project was supported by funds from National Institutes of Health Innovative Molecular Analysis Technologies Program (Grant #5R33CA177456), and a sponsored research grant with NetScientific.

References

1. Cristofanilli M, Budd T, Ellis MJ, Stopeck A, Matera J, Miller CM, Reuben JM, Doyle GV, Allard JW, Terstappen LWMM, Hayes DF. N Engl J Med. 2004; 351:781–791. [PubMed: 15317891]
2. Krebs MG, Sloane R, Priest L, Lancashire L, Hou JM, Greystoke A, Ward TH, Ferraldeschi R, Hughes A, Clack G, Ranson M, Dive C, Blackhall FH. J Clin Oncol. 2011; 29:1556–63. [PubMed: 21422424]
3. Alama A, Truini A, Coco S, Genova C, Grossi F. Drug Discov Today. 2014; 19:1671–1676. [PubMed: 24928031]
4. Alix-Panabières C, Pantel K. Nat Rev Cancer. 2014; 14:623. [PubMed: 25154812]
5. Bonnomet A, Brysse A, Tachsidis A, Waltham M, Thompson EW, Polette M, Gilles C. J Mammary Gland Biol Neoplasia. 2010; 15:261–273. [PubMed: 20449641]
6. Yu M, Bardia A, Wittner BS, Stott SL, Smas ME, Ting DT, Isakoff SJ, Ciciliano JC, Wells MN, Shah AM, Concannon KF, Donaldson MC, Sequist LV, Brachtel E, Sgroi D, Baselga J, Ramaswamy S, Toner M. Science. 2013; 339:580–584. [PubMed: 23372014]
7. Ozkumur E, Shah AM, Ciciliano JC, Emmink BL, Miyamoto DT, Brachtel E, Yu M, Chen P -i P, Morgan B, Trautwein J, Kimura A, Sengupta S, Stott SL, Karabacak NM, Barber Ta, Walsh JR, Smith K, Spuhler PS, Sullivan JP, Lee RJ, Ting DT, Luo X, Shaw AT, Bardia A, Sequist LV, Louis DN, Maheswaran S, Kapur R, Haber Da, Toner M. Sci Transl Med. 2013; 5:179ra47.
8. Darling EM, Di Carlo D. Annu Rev Biomed Eng. 2015; 17:35–62. [PubMed: 26194428]
9. Kiessling TR, Herrera M, Nnetu KD, Balzer EM, Girvan M, Fritsch AW, Martin SS, Käs JA, Losert W. Eur Biophys J. 2013; 42:383–394. [PubMed: 23504046]
10. Jin C, McFaul SM, Duffy SP, Deng X, Tavassoli P, Black PC, Ma H. Lab Chip. 2013; 14:32–44. [PubMed: 23963515]
11. Low WS, Abas WA, Wan B. Biomed Res Int. 2015; 2015:1–22.
12. Lee A, Park J, Lim M, Sunkara V, Kim SY, Kim GH, Kim M, Cho Y. Anal Chem. 2014; 86:11349–11356. [PubMed: 25317565]
13. Lin BK, McFaul SM, Jin C, Black PC, Ma H. Biomicrofluidics. 2013; 7:34114. [PubMed: 24404034]
14. Liu Z, Huang F, Du J, Shu W, Feng H, Xu X, Chen Y. Biomicrofluidics. 2013; 7:11801. [PubMed: 24396522]
15. Hou HW, Warkiani ME, Khoo BL, Li ZR, Soo Ra, Tan DS-W, Lim W-T, Han J, Bhagat AAS, Lim CT. Sci Rep. 2013; 3:1259. [PubMed: 23405273]
16. Di Carlo D. Lab Chip. 2009; 9:3038–46. [PubMed: 19823716]
17. Guck J, Schinkinger S, Lincoln B, Wottawah F, Ebert S, Romeyke M, Lenz D, Erickson HM, Ananthakrishnan R, Mitchell D, Käs J, Ulvick S, Bilby C. Biophys J. 2005; 88:3689–3698. [PubMed: 15722433]
18. Remmerbach TW, Wottawah F, Dietrich J, Lincoln B, Wittekind C, Guck J. Cancer Res. 2009; 69:1728–1732. [PubMed: 19223529]
19. Cross SE, Jin YS, Rao J, Gimzewski JK. Nat Nanotechnol. 2007; 2:780–3. [PubMed: 18654431]
20. Phillips KG, Kuhn P, McCarty OJT. Am J Physiol Cell Physiol. 2014; 306:C80–8. [PubMed: 24133063]
21. Bao G, Suresh S. Nat Mater. 2003; 2:715–725. [PubMed: 14593396]
22. Byun S, Son S, Amodei D, Cermak N, Shaw J, Kang JH, Hecht VC, Winslow MM, Jacks T, Mallick P, Manalis SR. Proc Natl Acad Sci U S A. 2013; 110:7580–5. [PubMed: 23610435]

23. Bagnall, J Shaw, Byun, S., Begum, S., Miyamoto, DT., Hecht, VC., Maheswaran, S., Stott, SL., Toner, M., Hynes, RO., Manalis, SR. Sci Rep. 2015; 5:18542. [PubMed: 26679988]
24. Otto O, Rosendahl P, Mietke A, Golfier S, Herold C, Klaue D, Girardo S, Pagliara S, Ekpenyong A, Jacobi A, Wobus M, Töpfner N, Keyser UF, Mansfeld J, Fischer-Friedrich E, Guck J. Nat Methods. 2015; 12
25. Dudani JS, Gossett DR, Tse HTK, Di Carlo D. Lab Chip. 2013; 13:3728–34. [PubMed: 23884381]
26. Yang T, Paiè P, Nava G, Bragheri F, Vazquez RM, Minzioni P, Veglione M, Tano M Di, Mondello C, Osellame R, Cristiani I. Lab Chip. 2015; 15:1262–1266. [PubMed: 25622755]
27. Runge J, Reichert TE, Fritsch A, Käs J, Bertolini J, Remmerbach TW. Oral Dis. 2014; 20:120–127.
28. Coughlin MF, Bielenberg DR, Lenormand G, Marinkovic M, Waghorne CG, Zetter BR, Fredberg JJ. Clin Exp Metastasis. 2013; 30:237–250. [PubMed: 22961212]
29. Mak M, Erickson D. Integr Biol. 2013; 5:1374–84.
30. Chen CL, Mahalingam D, Osmulski P, Jadhav RR, Wang CM, Leach RJ, Chang TC, Weitman SD, Kumar AP, Sun L, Gaczynska ME, Thompson IM, Huang THM. Prostate. 2013; 73:813–826. [PubMed: 23280481]
31. Gossett DR, Tse HTK, Lee Sa, Ying Y, Lindgren AG, Yang OO, Rao J, Clark AT, Di Carlo D. Proc Natl Acad Sci. 2012; 109:7630–5. [PubMed: 22547795]
32. Lekka M, Gil D, Pogoda K, Dulińska-Litewka J, Jach R, Gostek J, Klymenko O, Prauzner-Bechcicki S, Stachura Z, Wiltowska-Zuber J, Okoń K, Laidler P. Arch Biochem Biophys. 2012; 518:151–156. [PubMed: 22209753]
33. Tse HTK, Gossett DR, Moon YS, Masaeli M, Sohsman M, Ying Y, Mislick K, Adams RP, Rao J, Di Carlo D. Sci Transl Med. 2013; 5:212ra163.
34. Che J, Yu V, Dhar M, Renier C, Matsumoto M, Heirich K, Garon EB, Goldman J, Rao J, George W, Pegram MD, Sheth S, Jeffrey SS, Kulkarni RP, Sollier E, Di Carlo D. Oncotarget. 2016
35. Sollier E, Go DE, Che J, Gossett DR, O'Byrne S, Weaver WM, Kummer N, Rettig M, Goldman J, Nickols N, McCloskey S, Kulkarni RP, Di Carlo D. Lab Chip. 2014; 14:63–77. [PubMed: 24061411]
36. Chinen LTD, de Carvalho FM, Rocha BMM, Aguiar CM, Abdallah EA, Campanha D, Mingues NB, de Oliveira TB, Maciel MS, Cervantes GM, Dettino ALa, Soares FA, Paterlini-Bréchot P, Fanelli MF. J Thorac Dis. 2013; 5:593–599. [PubMed: 24255771]
37. Qin X, Park S, Duffy SP, Matthews K, Ang RR, Todenhöfer T, Abdi H, Azad A, Bazov J, Chi KN, Black PC, Ma H. Lab Chip. 2015; 15:2278–2286. [PubMed: 25876237]
38. Lekka M, Laidler P, Gil D, Lekki J, Stachura Z, Hrynkiewicz aZ. Eur Biophys J. 1999; 28:312–316. [PubMed: 10394623]
39. Zhang W, Kai K, Choi DS, Iwamoto T, Nguyen YH, Wong H, Landis MD, Ueno NT, Chang J, Qin L. Proc Natl Acad Sci U S A. 2012; 109:18707–12. [PubMed: 23112172]
40. Martinez Vazquez R, Nava G, Veglione M, Yang T, Bragheri F, Minzioni P, Bianchi E, Di Tano M, Chiodi I, Osellame R, Mondello C, Cristiani I. Integr Biol. 2015; 7:477–484.
41. Händel C, Schmidt BUS, Schiller J, Dietrich U, Möhn T, Kießling TR, Pawlizak S, Fritsch AW, Horn LC, Briest S, Höckel M, Zink M, Käs JA. New J Phys. 2015; 17:83008.
42. Jonas O, Mierke CT, Käs Ja. Soft Matter. 2011; 7:11488.
43. Basu R, Whitlock BM, Husson J, Floc'h A Le, Jin W, Oyler-Yaniv A, Dotiwala F, Giannone G, Hivroz C, Biais N, Lieberman J, Kam LC, Huse M. Cell. 2016; 165:1–11.
44. Suresh S. Acta Mater. 2007; 55:3989–4014.
45. Rotem A, Ram O, Shoresh N, Sperling RA, Goren A, Weitz DA, Bernstein BE. Nat Biotechnol. 2015; 33:1165–72. [PubMed: 26458175]
46. Lam, Wa, Rosenbluth, MJ., Fletcher, Da, Dc, W. 2009; 109:3505–3508.
47. Jain RK, Martin JD, Stylianopoulos T. Annu Rev Biomed Eng. 2014; 16:321–346. [PubMed: 25014786]
48. Mousavi M, Chen HY, Hou HS, Chang CYY, Roffler S, Wei PK, Cheng JY. Biosensors. 2015; 5:98–117. [PubMed: 25806834]
49. Pallaoro A, Hoonejani MR, Braun GB, Meinhart CD, Moskovits M. ACS Nano. 2015; 4:4328–4336.

50. Strohm EM, Kolios MC. Cytom Part A. 2015; 87:741–749.
51. Wang T, Liu J, gu X, Li D, Wang J, Wang E. Anal Chim Acta. 2015; 882:32–37. [PubMed: 26043089]
52. Wang C, Ye M, Cheng L, Li R, Zhu W, Shi Z, Fan C, He J, Liu J, Liu Z. Biomaterials. 2015; 54:55–62. [PubMed: 25907039]
53. Gu Y, Ju C, Li Y, Shang Z, Wu Y, Jia Y, Niu Y. Biosens Bioelectron. 2015; 66:24–31. [PubMed: 25460877]
54. Nwankire CE, Venkatanarayanan A, Glennon T, Keyes TE, Forster RJ, Ducrée J. Biosens Bioelectron. 2014; 68C:382–389.
55. Hardingham JE, Kotasek D, Robert E, Eaton MC, Pascoe VH, Ii AD. 1995; 1:789–794.
56. Zhao S, Yang H, Zhang M, Zhang D, Liu Y, Liu Y, Song Y, Zhang X, Li H, Ma W, Zhang Q. Cell Biochem Biophys. 2013; 65:263–273. [PubMed: 22990361]
57. Vedula SRK, Leong MC, Lai TL, Hersen P, Kabla AJ, Lim CT, Ladoux B. Proc Natl Acad Sci. 2012; 109:12974–9. [PubMed: 22814373]
58. Qi D, Hoelzle DJ, Rowat aC. Eur Phys J Spec Top. 2012; 204:85–101.
59. Chiu TK, Lei KF, Hsieh CH, Hsiao HB, Wang HM, Wu MH. Sensors. 2015; 15:6789–6806. [PubMed: 25808775]
60. Macosko EZ, Basu A, Satija R, Nemesh J, Shekhar K, Goldman M, Tirosh I, Bialas AR, Kamitaki N, Martersteck EM, Trombetta JJ, Weitz DA, Sanes JR, Shalek AK, Regev A, McCarroll SA. Cell. 2015; 161:1202–1214. [PubMed: 26000488]
61. Abbaspourrad A, Zhang H, Tao Y, Cui N, Asahara H, Zhou Y, Yue D, Koehler SA, Ung LW, Heyman J, Ren Y, Ziblat R, Chong S, Weitz DA. Sci Rep. 2015; 5:12756. [PubMed: 26234416]

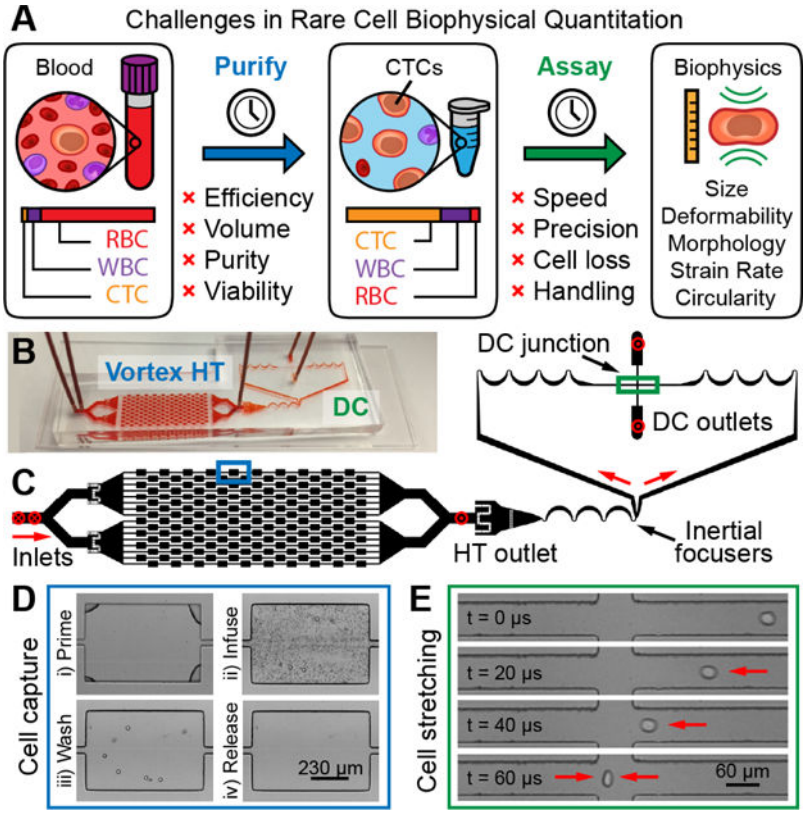

Fig. 1.

VDC device design and workflow for mechanophenotyping of rare cells. (A) Successful biophysical characterization of CTCs requires overcoming many challenges in the i) purification of CTCs and ii) ability to assay cells with high fidelity, all in a seamless workflow. (B) VDC is a glass-bonded PDMS device consisting of the Vortex HT cell capture region and a downstream DC region for subsequent cell mechanophenotyping. (C) The device contains 2 inlets for sample and wash buffer, and 3 outlets. Fluid waste passes through the HT outlet during cell capture, and enriched cells pass through an initial biasing inertial focuser and a final alignment inertial focuser to arrive centered at the DC junction from one side and then out the 2 DC outlets during cell release. (D) CTC capture in the vortex region consists of device priming, sample infusion, solution exchange, and cell release. (E) Upon release, cells pass through the DC junction, where high speed imaging records cell deformation. Cells are quickly stretched at the junction and exit through either of the 2 DC outlets for downstream collection and further analysis.

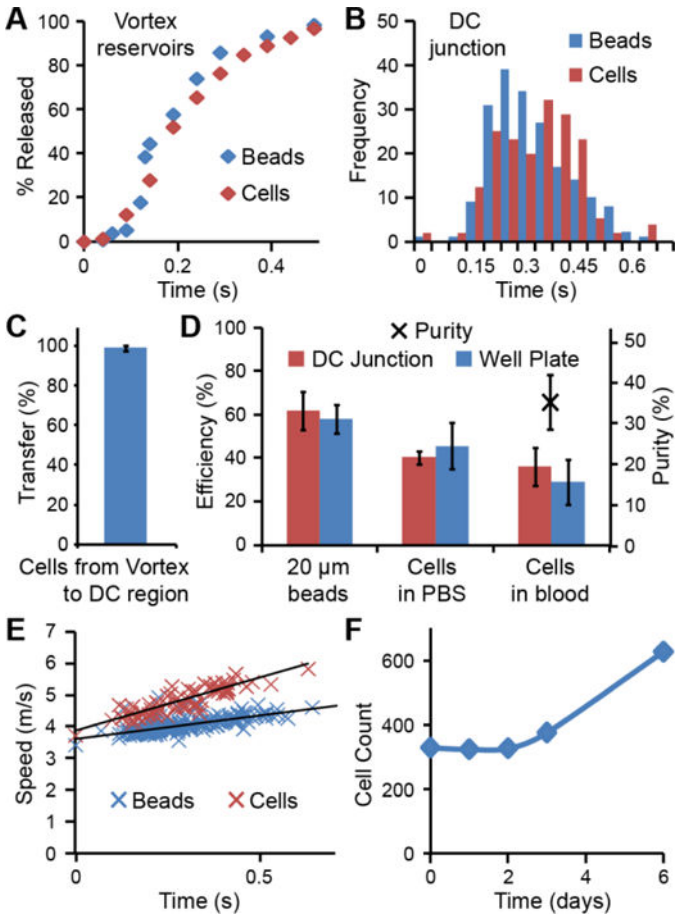

Fig. 2.

The combined Vortex-DC system can capture and release cells quickly and efficiently to realize high quality deformability measurements. (A) Captured beads and cells are released from vortices in a quick <0.5s time interval. (B) Particles also pass through the DC junction in a short time, <0.5s, which allows all cells to be imaged within the buffer capacity of the high speed camera. (C) Nearly all cells (98.7% ± 1.5%, n=4) pass through from the Vortex HT to DC region, indicating minimal cell loss between device regions. (D) VDC capture efficiency was calculated for 20µm diameter beads, MCF7 cells suspended in PBS buffer, and MCF7 cells spiked in 10× diluted healthy blood, counted from the DC junction (red, n=3) or the well plate (blue, n=3). (E) The speed of cells slightly increases over the course of their release, but is a high enough velocity to observe and resolve deformations, and does not bias measurements (see Fig. S6B). (F) Collected cells are still viable following VDC processing and may proliferate in culture for over 6 days.

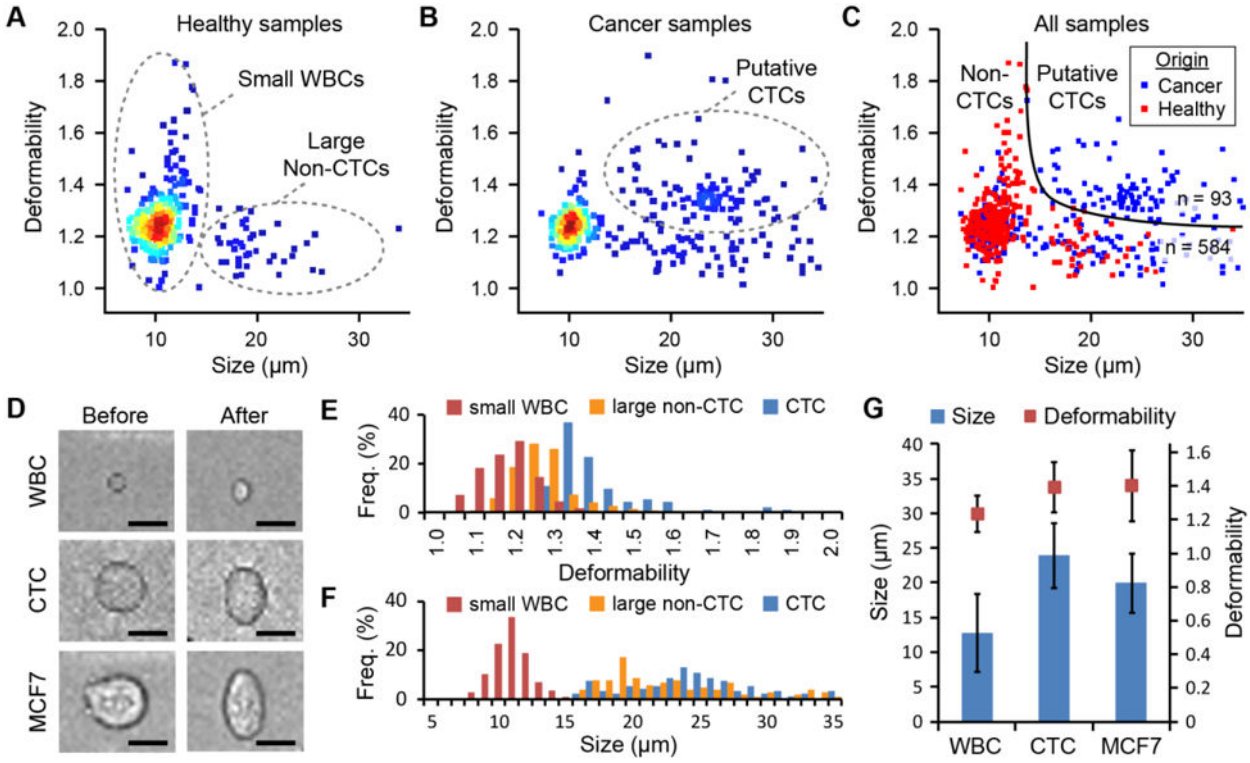

Fig. 3.

Non-small cell lung cancer (NSCLC) patients have more large and highly deformable cells in circulation. (A) Samples from 5 healthy volunteers were processed with VDC and revealed populations of smaller WBCs and larger circulating cells with low deformability. (B) Samples from 16 NSCLC patients revealed a unique population of large, deformable CTCs. (C) Setting a threshold using a support vector machine learning approach on cancer patient cells (blue) and healthy donor cells (red), 93 cells from all patients were identified as CTCs. (D) Examples of typical cells observed in high speed VDC videos before and after deformation. CTC populations were generally (E) more deformable (>1.3) and (F) larger (>15μm) than WBC populations. (G) CTCs also exhibited similar biophysical profiles as the MCF7 breast cancer cell line.

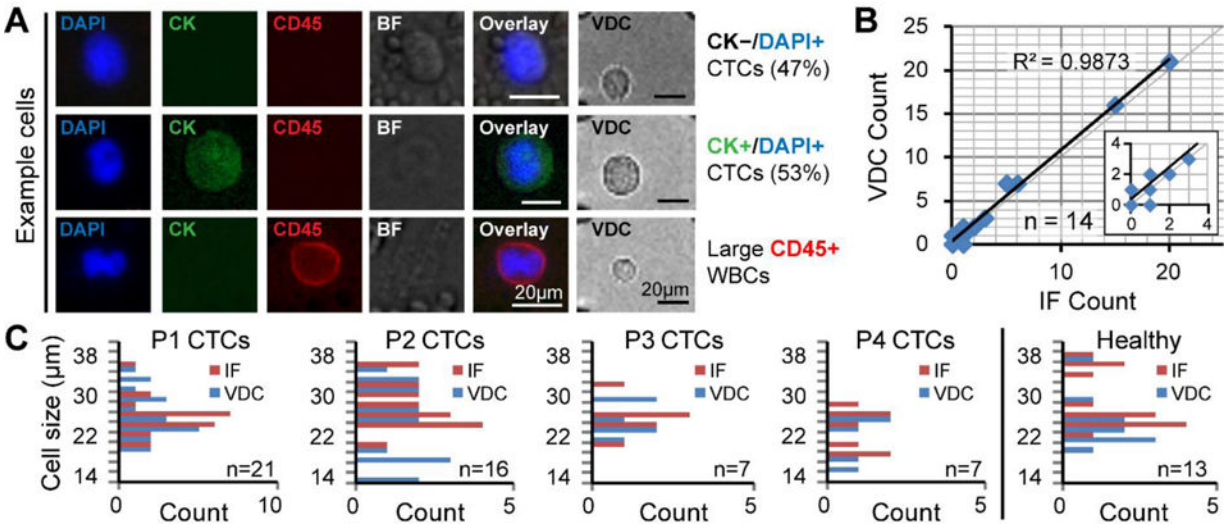

Fig. 4.

Comparisons of VDC with IF. (A) Similar to Vortex HT, VDC captured CTCs which stained both positive and negative for CK, as well as large white blood cells. (B) The number of CTCs defined from VDC matches closely with the number enumerated with the conventional IF technique (n=14 patients). (C) The size distributions of CTCs from each patient matched closely between VDC (blue) and IF (red). Here, n refers to total cell numbers per patient. Large WBCs observed in both techniques also appeared similar in size, as observed in one healthy patient (last graph).

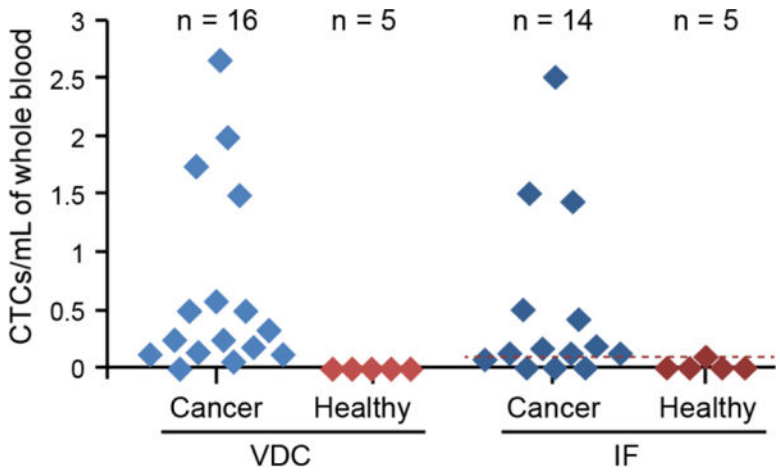

Fig. 5.

Biophysical enumeration of CTCs with VDC versus cytomorphological enumeration by IF. Biophysical enumeration of CTCs from 16 stage IV cancer samples revealed a 93.8% positive test rate using SVM thresholding, compared with a 71.4% positive rate using the gold standard IF technique, setting the highest cell count from healthy samples as a threshold (dotted red line).